Journal of ELECTRONIC MATERIALS, Vol. 47, No. 9, 2018
https://doi.org/10.1007/s11664-018-6468-2
© 2018 The Minerals, Metals & Materials Society

P-Type Characteristic of Nitrogen-Doped ZnO Films

ZI-NENG NG,[1] KAH-YOONG CHAN,[1,3] SHAHRUDDIN MUSLIMIN,[1] and DIETMAR KNIPP[2]

1.—Centre for Advanced Devices and Systems, Faculty of Engineering, Multimedia University, 63100 Cyberjaya, Selangor, Malaysia. 2.—Geballe Laboratory for Advanced Materials, Department of Materials Science and Engineering, Stanford University, Stanford, CA 94305, USA. 3.—e-mail: kychan@mmu.edu.my

Zinc oxide (ZnO) is a promising material for emerging electronic and photonic applications due to its wide direct band gap and large exciton binding energy. Despite on-going developments, the control of the conductivity type in ZnO films continues to be a challenge. Stable *p*-type ZnO is required in order to fabricate standalone ZnO-based devices. Nitrogen is considered as a promising candidate to produce a shallow acceptor level in ZnO, since it has similar radii and electrical structure to oxygen. In this experiment, we utilize the low cost sol–gel spin coating technique to fabricate nitrogen-doped ZnO (ZnO:N) films. All films show great optical transmittance above 80% in the visible region. ZnO:N film at 15 at.% doping concentration shows strong UV emission and exhibits low resistivity. A *p*–*n* homojunction device based on ZnO:N shows characteristic of a typical rectifying diode, with a turn-on voltage of approximately 1.2 V.

Key words: Zinc oxide, nitrogen-doping, *p*-type, sol–gel

INTRODUCTION

Zinc oxide (ZnO) holds a unique position among other semiconducting materials for its wide band gap, high transparency in the visible range, and good electrical conductivity. The ease of doping ZnO with donors such as aluminum (Al) and gallium (Ga) makes it a promising material as transparent conductive oxide (TCO), which is an essential component for sensors, solar cells, light emitting diodes (LEDs), and window coatings.[1–5] ZnO has the potential to contend against the current market dominant indium tin oxide (ITO).[6] Sophisticated fabrication methods for ZnO films are favorable, but come with higher maintenance and operation costs.[7–11] With such concerns, many researchers attempted to fabricate ZnO films with the sol–gel method and have been able to deliver promising results.[12–14] The challenge, however, is the realization of *p*-type ZnO materials with concerns such as strong self-compensation by intrinsic donor defects, deep acceptor level, and low solubility of *p*-type doping sources.[15]

Over the years, the fabrication of *p*-type ZnO has been attempted with acceptors namely arsenic (As), phosphorus (P), sodium (Na), silver (Ag), potassium (K), and nitrogen (N).[16–21] The generation of acceptor state based on the substitution with the oxygen (O)-site (O-site) can be done by incorporating group-VA impurities (As, P, and N). Among the group-VA impurities, nitrogen doping is believed to form *p*-type ZnO due to the similarity of ionic radius between N (1.68 Å) and O (1.38 Å) (only 22% larger than that of O).[15] However, the electrical conductivity of nitrogen-doped ZnO (ZnO:N) films remained controversial due to the low hole concentration and its instability to remain *p*-type. A number of works on ZnO:N films deposited using advanced physical deposition methods have been able to deliver promising results. In the works of Dhara et al. the annealed ZnO:N films grown using RF sputtering has managed to retained its *p*-type conductivity for up to 20 months, while the non-

(Received July 31, 2017; accepted June 19, 2018; published online June 29, 2018)

annealed films only lasted a few days before turning back to *n*-type.[22] Nagar et al. used plasma immersion ion implantation to dope N ions on sputtered ZnO films and were able to achieve stable *p*-type conductivity for a period of 9 months.[23] In an aqueous approach, Golshahi et al. confirmed that their pyrolytically sprayed ZnO:N films at substrate temperature of more than 450°C are *p*-type conducting.[24] Pathak et al. also reported *p*-type conductivity in their 2 and 3 at.% of their sol–gel spin coated ZnO:N films.[25] However, the aforementioned works are not consistent in terms of the nitrogen-doping concentration, some works have incorporated higher nitrogen-doping concentration, but are still able obtain promising results.[26] Therefore, more research should be done especially with a wet chemical/aqueous approach in order to confirm the effects of nitrogen-doping concentration.

In our approach, we utilized the easiness of incorporating ZnO with N acceptors (N_O) by sol–gel spin coating technique, with nitrogen-doping concentration from 0 to 30 at.%. The effects of nitrogen-doping concentration on the properties of the ZnO:N films were investigated. Hall Effect measurement was performed to verify the *p*-type characteristic of the samples. Further investigation was carried out by integrating ZnO:N film with *n*-type Al doped ZnO (ZnO:Al) film to form a *p*–*n* junction, which is characterized by current-voltage (I–V) measurement system.

EXPERIMENTAL

The ZnO solutions were prepared by a mixture of zinc acetate dihydrate as precursor, isopropanol as solvent, and monoethanolamine as stabilizer. Ammonium acetate was added to the ZnO solutions as the source of N_O. The resultant undoped ZnO and ZnO:N solutions with doping concentration of 5 at.%, 10 at.%, 15 at.%, 20 at.%, and 30 at.% were stirred at 60°C for 2 h and aged at room temperature for another 22 h. The solutions were then added dropwise onto the glass substrates and spin-coated at 3000 RPM. Finally, the samples underwent a post-annealing process at 450 °C. The thickness, morphological, structural, optical, photoluminescence (PL), and electrical properties of the ZnO films were characterized by surface profilometry, atomic force microscopy (AFM), x-ray diffractometry (XRD), ultraviolet-visible (UV–Vis) spectroscopy, PL spectroscopy, and Hall Effect, respectively. Finally, the ZnO:N film was integrated with *n*-type ZnO:Al to form a *p*–*n* junction device. The fabrication of the constituent ZnO:Al film, which is utilized in the realization of the p-n junction has been discussed in our previous work.[13] The I–V measurement was performed to verify the I–V characteristic of the device. The results are analyzed and presented in the following sections.

RESULTS AND DISCUSSION

Surface profilometer was used to measure the sol–gel spin coated intrinsic ZnO and ZnO:N films. The thickness of intrinsic ZnO film is slightly thicker at 240 nm, whereas doped films are approximately 165 nm to 192 nm, as plotted in Fig. 1. Since all spin coating parameters were fixed, i.e. spinning speed and number of layers, the thickness variation in doped films may be due to the viscosity of the sol, which may be affected by the incorporation of doping compound.[27] Next, the surface morphology of the films scanned by AFM is shown in Fig. 2. Densely packed granular structures can be observed on the surface of all samples. The increment of doping content did not alter the morphology significantly. The grain size distribution bar graph extracted by Gwyddion software (from the AFM images given Fig. 2 is shown Fig. 3.

The XRD diffractograms of the intrinsic ZnO and ZnO:N films are shown in Fig. 4. The peaks from the XRD diffractogram fit well with the wurtzite structure of hexagonal ZnO. Obviously, there is a tendency for crystal growth in the (0 0 2) orientation, which agrees well with our doped *n*-type ZnO films as reported previously.[13,28] Tiny peaks can be observed at 36° and 47° in Fig. 4 as well, which correspond to the diffraction peaks for (1 0 1) and (1 0 2), respectively. These XRD diffraction peaks are in agreement with the JCPDS card No. 36-1451. The *c*-axis orientation grew the fastest as ZnO display higher surface energy in (0 0 2) polar plane and lower energy in non-polar planes. With the self-ordering effect, the crystal surface free energy and the interaction between the film and the substrate surface were reduced.[29] However, the intensity of (0 0 2) peak decreases with the increase of doping content. The high doping concentration has reduced the O vacancies (V_O) in to the films, which leads to the change of crystallinity and structure of ZnO films.[30] The crystallite size, D was estimated using Scherrer's Eq. 1 based on (0 0 2) diffraction peak as shown below:

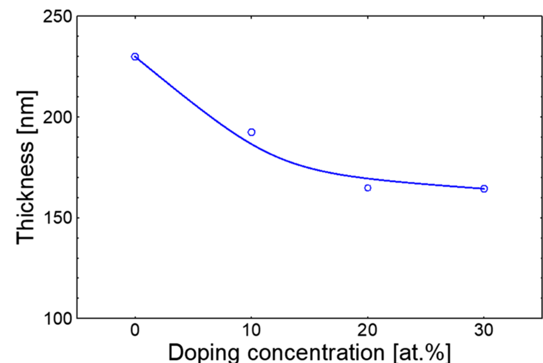

Fig. 1. Film thickness of ZnO:N films with respect to nitrogen-doping concentration.

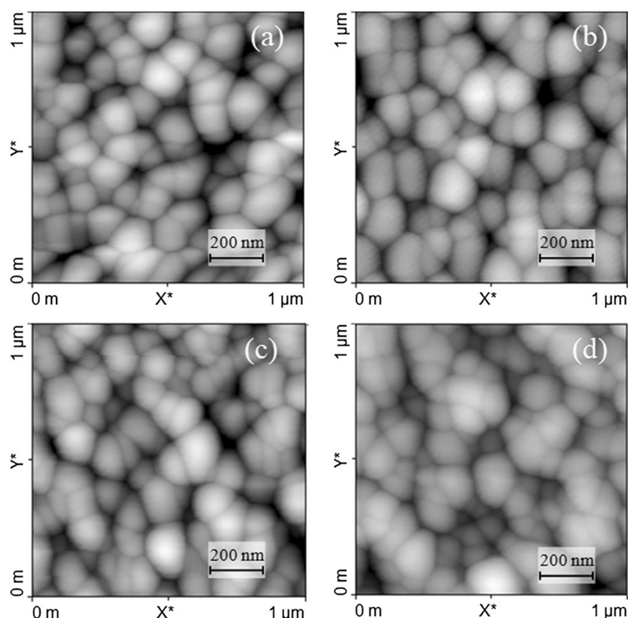

Fig. 2. Surface morphologies of (a) intrinsic ZnO, (b) ZnO:N 10 at.%, (c) ZnO:N 20 at.%, and (d) ZnO:N 30 at.% films.

$$D = \frac{0.9\lambda}{\beta \cos\theta} \quad (1)$$

where λ is the wavelength of incident x-ray (1.5406 Å), β is the FWHM, and θ is the Bragg's angle of the (0 0 2) diffraction peak. The formulated D is at average 42 nm for all samples, as plotted in Fig. 5. Also plotted in Fig. 5 is the 2θ and stress with respect to nitrogen-doping concentration. The (0 0 2) peak of intrinsic ZnO film is at 34.47°, but shifted to a lower angle of 34.45° as nitrogen-doping increased to 30 at.%. The slight peak shift towards lower angle suggests a raise of the lattice constant.[31] The shift in (0 0 2) peak towards the lower angle also suggests that the films are in the condition of tensile/compressive stress. According the Bragg's law, the decrease of diffraction angle will increase the d-spacing and introduce stress into the film. The d-spacing obtained from XRD is 2.6021 Å, 2.6024 Å, 2.6030 Å, and 2.6036 Å for ZnO:N films from 0 to 30 at.%, respectively. Next, the strain of the ZnO:N films can be determined by considering the lattice parameter, c_{film} based on the d-spacing obtained from the XRD result with Eq. 2 below:

$$c_{\mathrm{film}} = 2d \quad (2)$$

The calculated c_{film} increase from 5.204 Å to 5.207 Å with increasing nitrogen-doping concentration, which is of close approximation to the value of c_{bulk} of ZnO at 5.200 Å.[32] The strain, ε with reference to the bulk can be calculated using the Eq. 3 below:

$$\varepsilon = (c_{\mathrm{film}} - c_{\mathrm{bulk}})/c_{\mathrm{bulk}} \quad (3)$$

Next, the film stress, σ parallel to the film surface can be derived with Eq. 4 below:

$$\sigma = \frac{2C_{13}^2 - C_{33}(C_{11} + C_{12})}{2C_{13}} \times \varepsilon \quad (4)$$

The following value of elastic constants, C_{ij} for single-crystalline ZnO is used: C_{11} = 208.8, C_{33} = 213.8, C_{12} = 119.7, C_{13} = 104.2 Gpa.[32] The numerical relation of σ to the ε as shown in Eq. 5:

$$\sigma = -233\varepsilon(\mathrm{Gpa}) \quad (5)$$

As plotted in Fig. 5, the calculated σ of ZnO:N films from 0 to 30 at.% is – 0.185 Gpa, – 0.215 Gpa, – 0.266 Gpa, and – 0.324 Gpa, respectively. The negative value of σ implies that the all the films are under compressive stress. The slight increase of compressive stress may have partially caused by the increase in formation energy as N ions were successfully diffused into the ZnO crystal lattice and replaced O ions on O-sites, due to the larger ion radii of N than that of O.[21,33] Another cause of compressive stress may be related to the reduced thickness in doped films, as it is common for thinner film thickness to introduce higher strain/stress at the interface during annealing.[34] This effect is more apparent especially with film thicknesses smaller than 600 nm.[35]

In Fig. 6, the plotted optical transmittance of all samples revealed a characteristic absorption of ZnO at wavelength ranges below 380 nm, which is caused by the transitions of electron from the valence band to the conduction band.[36] As the doping concentration increases, the absorption of UV decreases. A similar phenomenon can be found in the work of Chongsri et al.[37] This may be caused by the slight variation in film thickness, as the incorporation of dopants may alter the viscosity of the precursor solution. The slight oscillations seen in the visible range may be due to the interference of the reflection/refraction of the light on transparent substrate and film surface, in which thicker films may cause stronger oscillation.[38] The optical transmittance of the visible light at 400 nm to 750 nm for all samples is above 80%. The optical band gap estimated using the Tauc method decreases from 3.28 eV to 3.27 eV as more nitrogen-doping is incorporated. When doped with donors, it is common to observe a widening of the band gap and blue-shift in the UV peak in comparison to the intrinsic ZnO, as seen in n-type ZnO:Al and ZnO:Ga films.[13] On the contrary, p-type ZnO films doped with acceptors have shown band gap reduction instead, revealing a red-shift in UV peak in comparison with intrinsic ZnO materials.[36] The conduction band edge of ZnO consists of 2s and 2p states of O and 4s states of Zn, only 2p states of O controls the valence band edge, as the contribution of 3d states of Zn is negligible.[39] The substitution of O ions with N ions during nitrogen-doping forms Zn-N bonds in the ZnO film. Since the electron negativity of O (3.44) is larger than that of N (3.04), the Zn-N band has smaller ionicity than that of the Zn-O band.

Fig. 3. Grain size distribution of (a) intrinsic ZnO, (b) ZnO:N 10 at.%, (c) ZnO:N 20 at.%, and (d) ZnO:N 30 at.% films.

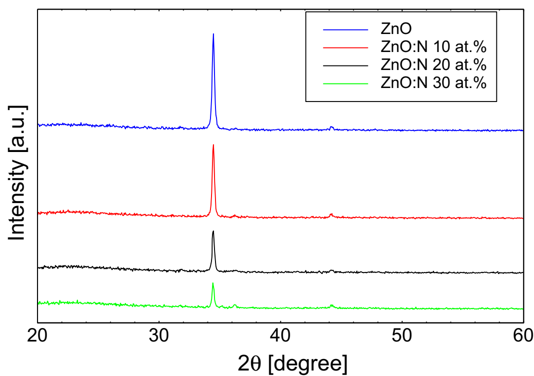

Fig. 4. XRD diffractogram of ZnO:N films with respect to nitrogen-doping concentrations.

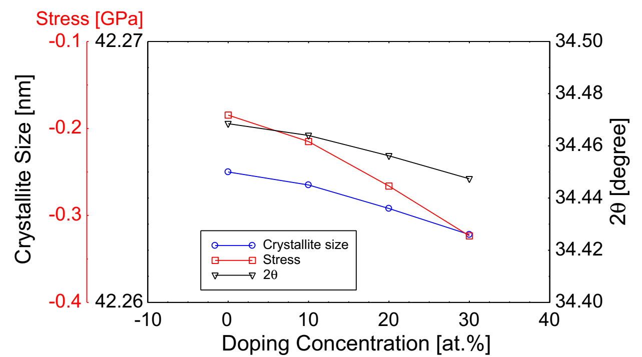

Fig. 5. Crystallite size, 2θ, and stress of ZnO:N films with respect to nitrogen-doping concentrations.

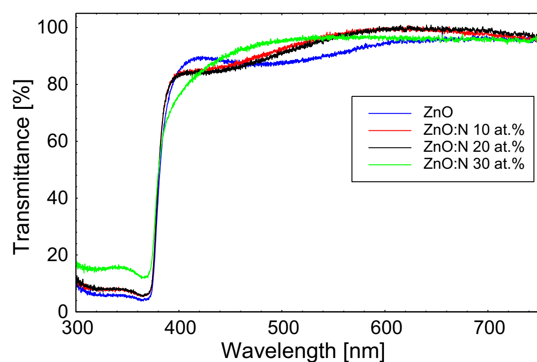

Fig. 6. Optical transmittances of ZnO:N films with respect to nitrogen-doping concentrations.

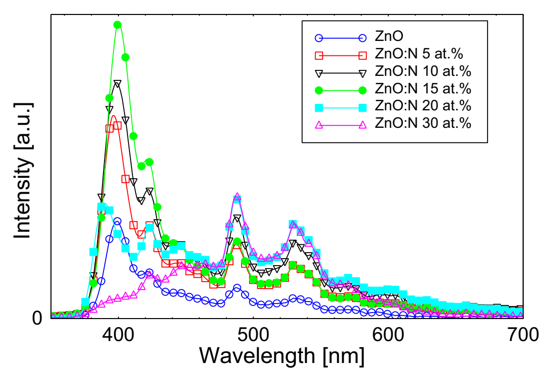

Fig. 7. PL spectra of ZnO:N films at various nitrogen-doping concentrations.

Hence, the decrease in band gap is probably due to the decrease in ionicity of Zn-N band in ZnO:N films.[40]

The PL spectra of the ZnO:N films is shown in Fig. 7. The UV emission at approximately 395 nm (3.15 eV) is the near-band-edge emission that originates from the free exciton recombination in ZnO.[41] Because of the insufficient holes in intrinsic ZnO film, its exciton concentration is restricted and resulted in lower UV peak.[42] However, the UV peak remains dominant and increases as nitrogen-doping increases to 15 at.%, upon successful doping of nitrogen into ZnO involves the substitution of a N ion for an O ion at one of the ZnO crystal lattice sites. The N ion serves as acceptor in the ZnO film and, therefore, has plenty of holes and excitons. The electrons could make it easily at the interface due to the shorter mean free path and the coulomb force based on quantum confinement effect.[43] Wang et al. reported an opposite trend on their ZnO:N films fabricated by filtered cathodic vacuum arc technique, which showed a decrease of UV emission intensity with an increase in nitrogen flow rate.[44] However, this can be justified by the lack of holes in their samples (which are still *n*-type, as reported). The UV emission peak decreases at 20 at.% and becomes less apparent at 30 at.%. A similar trend on UV emission was also observed in potassium doped ZnO films by Xu et al.[45] The quenching of intensity at higher doping concentration could also be caused by non-radiative Auger recombination processes linked to the degenerated electrons, in which an electron quickly absorbs the energy released by an electron recombination and gets dissipated by phonons.[46] The impurity clusters when nitrogen-doping concentration is high may also confine the radiative efficiency and cause the reduction of UV emission.[46] The relative PL intensity of visible bands is known for defect densities. The violet band emission shows a slight peak at approximately 423 nm (2.94 eV), which relates to the defect emission of Zn_i and Zn vacancies (V_{Zn}) associated with a deeper acceptor state. V_{Zn} is also commonly considered the dominant defect responding to the *p*-type conductivity.[41] A dominant peak located at 486 nm (2.55 eV), also known as deep-level emission, can be assigned to O-related defects.[47] It has been proposed that the deep-level emission is associated with individually ionized V_O and the recombination of a photogenerated hole with its charge state.[48] Another strong peak located at the green emission (530 nm) can be observed also. This type of emission is most commonly found in ZnO nanostructures, which is caused by the presence of V_O defects.[49,50]

Hall Effect measurement was performed to characterize the electrical properties of the ZnO:N films with various nitrogen-doping concentration. The square samples were prepared according to Van der Pauw method with Ag paste contacts at the corners. The measurement was repeated several times to confirm the carrier type of the samples. The resistivity, carrier concentration, and mobility of the films are plotted in Fig. 8. The type of carriers of the ZnO:N films determined Hall Effect were stated in the figure as well. ZnO:N films with 5 at.% to 30 at.% exhibited *p*-type characteristics. The Hall Effect result has clearly confirmed the incorporation of nitrogen into the ZnO film and production of *p*-type ZnO at nitrogen-doping concentration of 30 at.% and below. The plot shows a decrement in resistivity from the undoped sample to 15 at.% nitrogen-doping concentration at 57 Ω cm. The same sample also shows highest carrier density of 8.73×10^{16} cm^{-3} and Hall mobility at 1.25 $cm^2 V^{-1} s^{-1}$. The ZnO crystal is attributed as *n*-type non-stoichiometric semiconductor caused by V_O or excess Zn atoms. At 15 at.% nitrogen-doping concentration, the substitution of N ions with O ions in O-site produces N_O in the ZnO crystal lattice sites, which resulted in sufficient holes that dominate the intrinsic *n*-type defects.[51] However, the resistivity increases when nitrogen-doping concentration further increases to 30 at.%. At high nitrogen-doping concentration, the compensation of N_O occurs as the excess of N atoms may lead to the substitution of N_2 in O-sites [$(N_2)_O$] and formation of N_O-N_2 complexes, which behave as double shallow

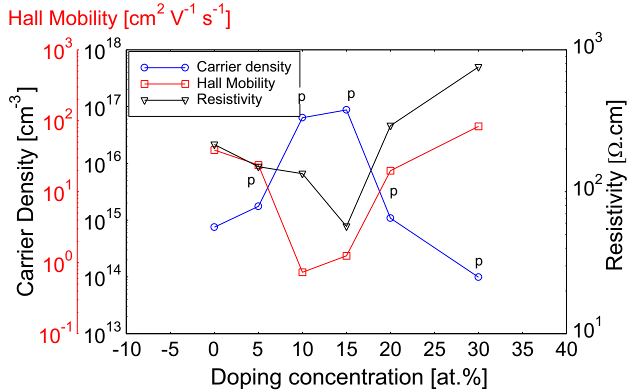

Fig. 8. Electrical properties of ZnO:N films with respect to nitrogen-doping concentrations.

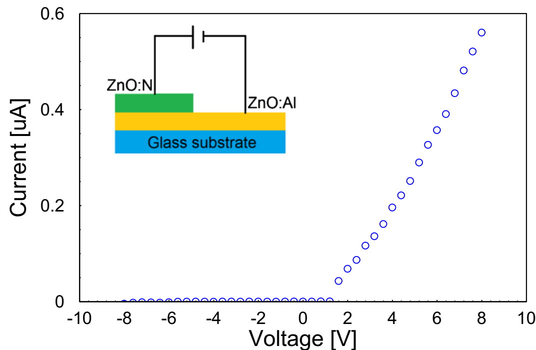

Fig. 9. I–V measurement of *p*-type ZnO:N/*n*-type ZnO:Al *p–n* junction (inset: *p–n* junction schematic structure).

donor and single donor, respectively.[39] Furthermore, the excess of N atoms may be incorporated in the interstitial site as donor defects and compensate for the shallow acceptors in the crystal lattice leading to an increase of electrical resistivity.[25] The decrease of mobility in 15 at.% nitrogen-doping concentration may be due to the increase of ionized impurity scattering mobility. In many cases, the ionized impurity scattering mobility is inversely proportional to the carrier concentration, as more carriers will result in an increase number of collisions and decrease the mobility of the holes.[52,53] ZnO:N film at 30 at.% nitrogen-doping concentration has the lowest carrier density and highest mobility. It is believed that the mechanism behind the high mobility is also related to the nanocrystal structure of polycrystalline ZnO films grown by aqueous method.[54] The high mobility of *p*-type doped ZnO films by fabricated by sol–gel method has also been reported in various works by Nian et al., Kalyanaraman et al., Park et al., and Wang et al. with mobility reported as high as 198 cm^2 V^{-1} s^{-1}.[55–58]

In order to verify the *p*-type characteristic of the ZnO:N films, the ZnO:N film was integrated with *n*-type ZnO:Al film to form a p-n junction on a 1″ × 0.5″ glass substrates, as shown in the inset of Fig. 9. The I-V characterization of the *p–n* junction was carried out by sweeping the input voltage from − 8 V to 8 V. The I–V curve plotted in Fig. 9 reveals the characteristics of typical *p–n* junctions. The plot shows a turn-on voltage of 1.2 V under forward biased voltage with no breakdown voltage observed in the I–V measurement range.

CONCLUSION

P-type ZnO:N films were successfully deposited using sol–gel spin coating technique. The AFM revealed hexagonal granular structure surface on all films, with only slight changes on the morphology. The XRD revealed a sharp (0 0 2) peak of hexagonal ZnO crystal structure, indicates good *c*-axis orientation as perpendicular to the substrate. The optical transmittance in the visible range of all films is in the range of 80% to 90% with estimated optical band gap of ZnO:N films ranges from 3.27 eV to 3.28 eV. At 15 at.% nitrogen-doping concentration, strong UV emission on PL spectra and lowest resistivity with *p*-type conductivity on Hall measurement were obtained. The ZnO:N/ZnO:Al *p–n* junction revealed a typical rectifying characteristic, with a turn-on voltage of approximately 1.2 V. The ZnO:N films in this work has shown promising properties for the application of optoelectronics.

ACKNOWLEDGEMENTS

This project is funded by Malaysian Ministry of Higher Education (MOHE)'s Fundamental Research Grant Scheme (Project Code: FRGS/1/2014/TK03/MMU/02/1). The authors would like to thank MOHE for the financial support and Multimedia University for providing the facilities for this research work.

REFERENCES

1. H. Zhou, D. Yi, Z. Yu, L. Xiao, and J. Li, *Thin Solid Films* 515, 6909 (2007).
2. E. Fortunato, L. Raniero, L. Siva, A. Gonçalves, A. Pimentel, P. Barquinha, H. Águas, L. Pereira, G. Gonçalves, I. Ferreira, E. Elangovan, and R. Martins, *Sol. Energy Mater. Sol. Cells* 92, 1605 (2008).
3. Y.S. Choi, J.W. Kang, D.K. Hwang, S.J. Park, and I.E.E.E. Trans, *Electron Devices* 57, 26 (2010).
4. M. Kashif, M.E. Ali, S.M.U. Ali, and U. Hashim, *Ceram. Int.* 39, 6461 (2013).
5. C.F. Lin, M.S. Lin, C.C. Chen, P.H. Tsai, and F.H. Wang, *Surf. Coatings Technol.* 231, 161 (2013).
6. R. Mariappan, V. Ponnuswamy, and P. Suresh, *Superlattices Microstruct.* 52, 500 (2012).
7. H. Kumarakuru, D. Cherns, and G.M. Fuge, *Surf. Coatings Technol.* 205, 5083 (2011).
8. H.X. Chen, J.J. Ding, X.G. Zhao, and S.Y. Ma, *Phys. B Condens. Matter* 405, 1339 (2010).
9. D. Kim, I. Yun, and H. Kim, *Curr. Appl. Phys.* 10, S459 (2010).
10. T. Prasada Rao and M.C. Santhosh Kumar, *J. Alloys Compd.* 506, 788 (2010).
11. S. Kuprenaite, T. Murauskas, A. Abrutis, V. Kubilius, Z. Saltyte, and V. Plausinaitiene, *Surf. Coatings Technol.* 271, 156 (2015).

12. R. Vettumperumal, S. Kalyanaraman, and R. Thangavel, *J. Mol. Struct.* 1059, 61 (2014).
13. Z.N. Ng, K.Y. Chan, C.Y. Low, S.A. Kamaruddin, and M.Z. Sahdan, *Ceram. Int.* 41, S254 (2015).
14. R. Ebrahimifard, M.R. Golobostanfard, and H. Abdizadeh, *Appl. Surf. Sci.* 290, 252 (2014).
15. V. Avrutin, D.J. Silversmith, and H. Morkoç, *Proc. IEEE* 98, 1269 (2010).
16. L.-W. Weng, W.-Y. Uen, S.-M. Lan, S.-M. Liao, T.-N. Yang, C.-H. Wu, H.-F. Hong, W.-Y. Ma, and C.-C. Shen, *Appl. Surf. Sci.* 277, 1 (2013).
17. F.X. Xiu, Z. Yang, L.J. Mandalapu, J.L. Liu, and W.P. Beyermann, *Appl. Phys. Lett.* 88, 1 (2006).
18. S.S. Lin, J.G. Lu, Z.Z. Ye, H.P. He, X.Q. Gu, L.X. Chen, J.Y. Huang, and B.H. Zhao, *Solid State Commun.* 148, 25 (2008).
19. M.Y. Tan, C.B. Yao, X.Y. Yan, J. Li, S.Y. Qu, J.Y. Hu, W.J. Sun, Q.H. Li, and S. Bin Yang, *Opt. Mater. (Amst).* 51, 133 (2016).
20. W. Jun and Y. Yintang, *Mater. Lett.* 62, 1899 (2008).
21. W.W. Liu, Z.Z. Zhang, B. Yao, D.Z. Shen, and C.L. Liu, *Opt. Mater. (Amst).* 35, 2486 (2013).
22. S. Dhara and P.K. Giri, *Thin Solid Films* 520, 5000 (2012).
23. S. Nagar and S. Chakrabarti, *Superlattices Microstruct.* 75, 9 (2014).
24. S. Golshahi, S.M. Rozati, A.M. Botelho do Rego, J. Wang, E. Elangovan, R. Martins, and E. Fortunato, *Mater. Sci. Eng. B* 178, 103 (2013).
25. T.K. Pathak, V. Kumar, H.C. Swart, and L.P. Purohit, *Phys. B Condens. Matter* 480, 31 (2016).
26. S.S. Shinde, C.H. Bhosale, and K.Y. Rajpure, *J. Photochem. Photobiol. B Biol.* 113, 70 (2012).
27. Q. Li, X. Li, and J. Zhang, *J. Alloys Compd.* 572, 175 (2013).
28. Z.-N. Ng, K.-Y. Chan, Y.-K. Sin, F.-K. Yam, and D. Knipp, *J. Nanosci. Nanotechnol.* 17, 348 (2017).
29. Z.Q. Xu, H. Deng, Y. Li, Q.H. Guo, and Y.R. Li, *Mater. Res. Bull.* 41, 354 (2006).
30. K. Shtereva, V. Tvarozek, I. Novotny, J. Kovac, P. Sutta, and A. Vincze, in *2006 25th International Conference Microelectronics MIEL 2006 - Proceedings* (IEEE, 2006), pp. 357–360.
31. L. Duan, W. Zhang, X. Yu, Z. Jiang, L. Luan, Y. Chen, and D. Li, *Appl. Surf. Sci.* 258, 10064 (2012).
32. M. Chen, Z.L. Pei, X. Wang, C. Sun, and L.S. Wen, *J Vac Sci Technol A Vacuum Surfaces Film* 19, 963 (2001).
33. X.-W. Zhao, X.-Y. Gao, X.-M. Chen, C. Chen, and M.-K. Zhao, *Chin. Phys. B* 22, 024202 (2013).
34. B. Houng, C.-L. Huang, and S.-Y. Tsai, *J. Cryst. Growth* 307, 328 (2007).
35. S. Al-Khawaja, B. Abdallah, S. Abou Shaker, and M. Kakhia, *Interfaces* 22, 221 (2015).
36. S. Khosravi-Gandomani, R. Yousefi, F. Jamali-Sheini, and N.M. Huang, *Ceram. Int.* 40, 7957 (2014).
37. K. Chongsri, S. Boonruang, W. Techitdheera, and W. Pecharapa, *Mater. Lett.* 65, 1842 (2011).
38. A. Valour, F. Cheviré, F. Tessier, F. Grasset, B. Dierre, T. Jiang, E. Faulques, L. Cario, and S. Jobic, *Solid State Science* (Amsterdam: Elsevier Masson, 2016), pp. 30–36.
39. H.T. Chang and G.J. Chen, *Thin Solid Films* 618, 84 (2016).
40. G. Yuan, Z. Ye, L. Zhu, Y. Zeng, J. Huang, Q. Qian, and J. Lu, *Mater. Lett.* 58, 3741 (2004).
41. R. Swapna and M.C. Santhosh Kumar, *Mater. Sci. Eng. B Solid-State Mater. Adv. Technol.* 178, 1032 (2013).
42. L. Duan, W. Zhang, X. Yu, P. Wang, Z. Jiang, L. Luan, Y. Chen, and D. Li, *Solid State Commun.* 157, 45 (2013).
43. I.S. Kim, E.K. Jeong, D.Y. Kim, M. Kumar, and S.Y. Choi, *Appl. Surf. Sci.* 255, 4011 (2009).
44. Y.G. Wang, S.P. Lau, X.H. Zhang, H.W. Lee, H.H. Hng, and B.K. Tay, *J. Cryst. Growth* 252, 265 (2003).
45. L. Xu, X. Li, and J. Yuan, *Superlattices Microstruct.* 44, 276 (2008).
46. X.B. Wang, C. Song, K.W. Geng, F. Zeng, and F. Pan, *Appl. Surf. Sci.* 253, 6905 (2007).
47. T.K. Pathak, V. Kumar, H.C. Swart, and L.P. Purohit, *Phys. E Low-Dimensional Syst. Nanostructures* 77, 1 (2016).
48. A. Sáaedi, R. Yousefi, F. Jamali-Sheini, M. Cheraghizade, and A. Khorsand, Zak, and N. M. Huang. *Superlattices Microstruct.* 61, 91 (2013).
49. Z. Ye, T. Wang, S. Wu, X. Ji, and Q. Zhang, *J. Alloys Compd.* 690, 189 (2017).
50. L.W. Wang, F. Wu, D.X. Tian, W.J. Li, L. Fang, C.Y. Kong, and M. Zhou, *J. Alloys Compd.* 623, 367 (2015).
51. M.B. Islam, M.M. Rahman, M.K.R. Khan, M.A. Halim, M.A. Sattar, D.K. Saha, and M.A. Hakim, *Thin Solid Films* 534, 137 (2013).
52. J. Millman and A. Grabel, *Microelectronics* (New York: McGraw-Hill, 1987).
53. J.G. Lu, Y.Z. Zhang, Z.Z. Ye, L.P. Zhu, L. Wang, B.H. Zhao, and Q.L. Liang, *Appl. Phys. Lett.* 88, 222114 (2006).
54. J.-L. Zhao, X.-M. Li, J.-M. Bian, W.-D. Yu, and C.-Y. Zhang, *J. Cryst. Growth* 280, 495 (2005).
55. H. Nian, S.H. Hahn, K.K. Koo, E.W. Shin, and E.J. Kim, Sol-Gel Derived N-Doped ZnO Thin Films. *Mater. Lett.* 63, 2246 (2009).
56. S. Kalyanaraman, R. Thangavel, and R. Vettumperumal, *J. Phys. Chem. Solids* 74, 504 (2013).
57. C. Park, S. Kim, and S. Lim, *Solid State Commun.* 167, 18 (2013).
58. D. Wang, J. Zhou, and G. Liu, *J. Alloys Compd.* 481, 802 (2009).